Citation
Li, Z. and Chen, L. and Fang, Q. and Chen, W. and Hao, H. and Zhu, R. and Zheng, K. 2019. Experimental and numerical study on CFRP strip strengthened clay brick masonry walls subjected to vented gas explosions. International Journal of Impact Engineering. 129: pp. 66-79. http://doi.org/10.1016/j.ijimpeng.2019.02.013

Experimental and Numerical Study on CFRP Strip Strengthened Clay Brick Masonry Walls Subjected to Vented Gas Explosions

Zhan Li [a], Li Chen [a,*], Qin Fang [a], Wensu Chen [b], Hong Hao [b,c], Rong Zhu [a], Kang Zheng [a]

[a] State Key Laboratory of Disaster Prevention & Mitigation of Explosion & Impact, Army Engineering University of PLA, Nanjing, Jiangsu 210007, China

[b] Centre for Infrastructure Monitoring and Protection, School of Civil and Mechanical Engineering, Curtin University, Australia

[c] School of Civil Engineering, Guangzhou University, Guangzhou, China

Abstract

A total of nine full-scale field blast tests were conducted in a specially designed reinforced concrete (RC) chamber to investigate the performance of carbon fiber reinforced polymer (CFRP) strip strengthened clay brick masonry walls subjected to vented gas explosions. Three wall specimens, i.e. unstrengthened, strengthened with distributed layout and strengthened with concentrated layout were prepared for blast tests. The testing data including overpressure time histories of vented gas explosions, displacement time histories, damage modes of each wall specimen were recorded and analyzed. It was found that under vented gas explosions, the wall specimen strengthened with concentrated layout showed improved blast resistance and all three wall specimens experienced typical flexural damage. Detailed micro models for masonry walls were developed in LS-DYNA, incorporating material parameters obtained from material tests. The accuracy of numerical models in predicting the responses of masonry walls was validated with the testing data. Parametric studies were conducted to explore the performances of masonry walls with different heights and thicknesses under blast loads specified by design codes. It was found that with the increase of wall thickness or the decrease of wall height, the maximum displacement and damage level of masonry walls decreased significantly. The 115mm-thick masonry walls needed be strengthened to prevent collapse under the specified blast loads. The strengthened walls experienced typical flexural response and the strengthening effectiveness of using CFRP, GFRP and spray-on polyurea were numerically compared.

Keywords: Clay brick; Masonry wall; CFRP strip; Vented gas explosion; Field test; Numerical simulation

1 Introduction

Masonry wall has been widely used as infill walls in reinforced concrete (RC) frame buildings. Due to the low tensile/shear strength of brick and bonding materials, unreinforced masonry infill wall is one of the most vulnerable components in the frame structures under out-of-plane loads. In order to improve its resistance capacity, externally bonding FRP composites is widely used in the engineering practice to retrofit the masonry walls [1, 2]. Meanwhile, with the popularization of natural gas used in the industrial and civilian fields, gas explosion accidents have been reported frequently. In order to reduce the potential hazards to lives and properties, it is necessary to investigate the performances of FRP strengthened masonry walls under gas explosions.

The performance of FRP strengthened masonry walls subjected to static out-of-plane loads was studied by many researchers. Hamoush et al. [3] studied the effectiveness of using GFRP web fabric and unidirectional fabric on strengthening concrete masonry unit (CMU) walls under uniformly distributed loads by using airbag. The construction workmanship was proposed for the retrofitting of unreinforced masonry walls to produce sufficient bond at the interface between CMU and composites. Hamilton and Dolan [4] studied four short (1.8 m high) and two tall (4.6 m high) CMU walls strengthened by GFRP composite under uniformly distributed static loads by using airbag and conducting theoretical analysis. Two types of failure modes, i.e. fracture and combination of fracture and delamination were identified. It was reported that the concentrated strain caused the fracture of GFRP and the localized debonding in the mid-span area relieved the concentrated effect of GFRP strips. Albert et al. [5] conducted four point bending tests on ten CMU walls strengthened with GFRP sheet, CFRP strap and CFRP sheet. It was concluded that applying FRP increased the strength and ductility of wall specimens significantly. The composite types, layers of FRP, axial loads, cyclic loads influenced the stiffness of specimens while the layout has effect on the local behavior. Bui and Limam [6] carried out full scale tests on hollow CMU walls strengthened with CFRP composite under out-of-plane static loads by using water bags. The change of failure modes and the enhancement of bearing capacity were observed. The results showed that the change of boundary condition affected the effectiveness of strengthening system significantly. Al-Salloum et al. [7, 8] studied the performance of CMU walls strengthened with GFRP laminates under out-of-plane static loads (i.e. concentrated line loads and uniformly distributed loads from airbag) and developed the analytical model for different loads. The analytical model was validated by comparing with the testing results of 47 specimens and design suggestions were also proposed for engineering practice. Hrynyk et al. [9, 10] carried out a series of tests on GFRP and spray-on polyurea strengthened clay brick and CMU walls by using airbag and the corresponding analytical approach was proposed and verified. It was reported that using GFRP-polyurea was superior to using spray-on polyurea only in improving load carrying capacity and energy dissipation of wall specimens and necessary anchorage is required between the composites and surrounding structures. Strengthening the unreinforced masonry walls with externally bonded composite material increases load carrying capacity and ductility of masonry walls significantly. The existing studies provide useful design and construction guides for engineering practice.

With the potential hazards from terrorist attacks, conventional weapons and accidental explosions, the retrofitting performance of masonry walls under blast loads attract attentions of researchers. In order to investigate the design of strengthened CMU masonry walls by using FRPs under high explosive loads, Myers et al. [11, 12] and Urgessa et al. [13] conducted field tests and single degree of freedom (SDOF) analysis. Based on the testing and analytical results, design procedure and guideline were proposed for the retrofitting of masonry walls. Besides CMU blocks, clay bricks, air entrained concrete (AEC) blocks and other types of masonry materials were used in the construction of masonry wall. The changes of masonry blocks with various strength, dimension, density and Young's' modulus also result in different performance of masonry walls under blast loads. Tan and Patoary [14] carried out full-scale tests and SDOF analyses on FRP strengthened solid clay brick masonry walls under TNT explosions. The design procedures were proposed, however no visible crack and debonding was observed in all specimens due to the low blast overpressure generated from the tests. Chen et al. [15, 16] carried out a series of blast tests on 1/2 scale masonry walls with CFRP strips, steel mesh and steel laminated sheets. Both the field tests and the numerical simulations proved that the steel mesh provided the best retrofitting efficacy owing to its good ductility and CFRP strips suffered shear failure at the boundaries of masonry walls. Muszynski et al. [17] reported the blast tests on the AEC masonry walls with dimensions of 2.81m long × 2.60 m high × 0.20 m wide. It was found that CFRP retrofitting was capable of significantly improving the blast resistance of masonry walls.

Owing to the rapid development of numerical simulation technology, more and more reliable numerical simulations are used to study retrofitting techniques for masonry structures under blast loads. Based on DYNA3D software, Davidson et al. [18, 19] developed detailed dynamic finite element models to study the damage and failure mechanisms of polymer-reinforced CMU walls. Alsayed et al. [20]

conducted field blast tests and numerical study on the GFRP sheet strengthened infill CMU masonry walls under C4 charge explosions by using ANSYS/AUTODYN. Explicit boundary modelling was used to simulate the interaction with supports, which may result in membrane effect and enhance the resistance of structures [18, 20, 21]. In order to improve the computational efficiency, the homogenized material model was employed for masonry walls and the composites were simulated as shell elements to reduce element number and the discrepancy between element sizes [20].

In general, the application of composite material enhances the equivalent section area of masonry walls, increases the stiffness significantly and in turn reduces the deflection of wall structures. The adhesive between composites and masonry blocks can mitigate the number of fragments and effectively reduce the threats from flying debris under blast loads [1]. All the above-mentioned studies focused on dynamic performances of masonry structures under blast loads generated by high explosives. The study of masonry walls subjected to gas explosion is very limited in the open literature. It is worth noting that the blast loads generated by gas explosions have very different characteristics such as lower amplitude, longer rise time, longer duration and possibly multiple peaks [22, 23]. As compared to those by high explosives, the performance of FRP strengthened masonry walls subjected to blast loads from gas and high-explosive explosions could be very different. Therefore, it is necessary to study the masonry wall responses to gas explosion for reliable predictions of the masonry wall damages and better design of protection measures for such walls to resist accidental gas explosions. In the previous studies [24-26], the performance and strengthening effectiveness by using FRP materials of AAC masonry walls under vented gas explosions were examined and discussed. As for the unreinforced clay brick masonry walls, only the response of unstrengthened clay brick masonry walls under gas explosions were studied by conducting full-scale field tests and numerical simulations.

In this study, a series of full scale field tests on CFRP strip strengthened clay brick masonry walls under vented gas explosions were conducted. The effect of strip layout (i.e. distributed layout and concentrated layout) on the performance of wall specimens were observed and discussed. A detailed micro model was also developed to reproduce the behavior of unreinforced and CFRP strengthened masonry walls by using LS-DYNA 971. The predictions from the numerical simulations were compared with the testing data to validate the numerical model. The verified numerical model was then used to study the performance and strengthening methods of masonry walls under blast loads specified by design codes.

2 Field blast tests

2.1 Preparation of wall specimens

According to the Chinese standard (GB50003-2011) [27], three wall specimens including one unstrengthened specimen and two strengthened specimens were prepared in the precast RC frames. All the wall specimens with the dimensions of 3.0 m × 2.0 m × 0.115 m were laid in Running pattern， as shown in Fig. 1. The dimensions of clay bricks used in the wall specimens were 240 mm length ×115 mm width ×90 mm height and the mortar, which was composed of cement, water and river sand in the weight ratio of 1: 6.8: 5.23, was 10 mm thick. The specimens were designed as one-way walls with the right and left boundaries separated from the RC frame by using two layers of 2 mm-thick plastic film.

Unidirectional CFRP strips (Toray Industry UT-70-30) with a unit weight of 300 g/m^2 were used to strengthen wall specimens. As provided by the supplier, the tensile strength of dry fiber was 4100 MPa and the nominal thickness of the fiber was 0.167 mm. The corresponding density of carbon fiber was 1.8 g/cm^3. The width of CFRP strips was 50 mm. Two strip layouts (i.e. distributed layout and concentrated layout) were used to strengthen wall specimens, as shown in Fig. 1. In the distributed layout, seven strips were evenly distributed at a distance of 250 mm along the vertical direction of wall specimens and eleven strips along the transverse direction of wall specimens at a distance of 250 mm, as shown in Fig. 1(b). The concentrated layout, which was designed by using the OptiStruct module of the software HYPERWORKS[28-30], consumed the same amount of CFRP strips as the distributed layout and the converged optimization result of the strengthening material density is shown in Fig. 2. In the concentrated layout, the CFRP strips were placed at an equal distance of 100 mm along both the vertical and transverse directions of the mid-span area, as shown in Fig. 1(c).

The epoxy resin consisting of two components (i.e. main agent and hardener) with a ratio of 2:1 was used as bonding agent for FRP application. The epoxy resin had a tensile strength of 42 MPa, tensile modulus of 2.7 GPa and rupture tensile strain of 1.6%. The ends of CFRP strips were fixed onto the RC frames by using angle irons.

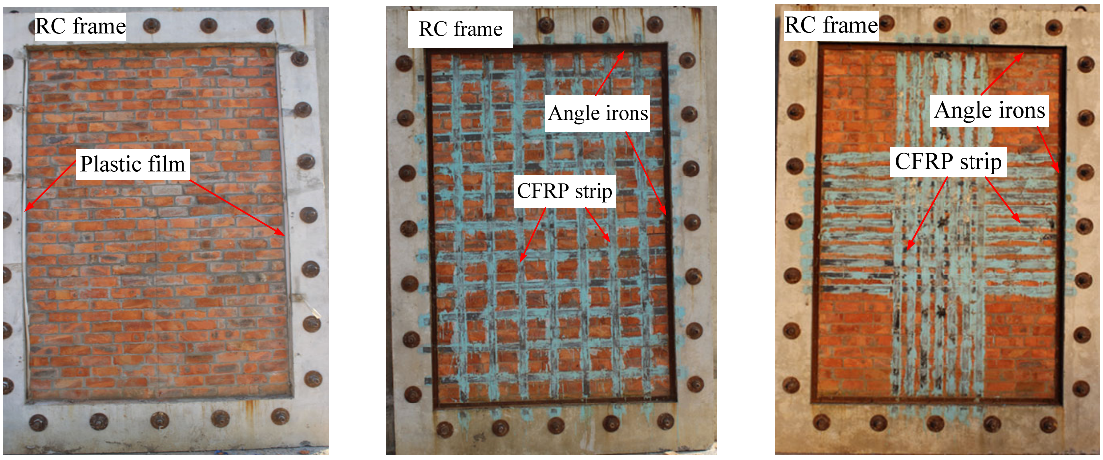

(a) Unstrengthened (b) Distributed layout (c) Concentrated layout

Fig. 1 Wall specimens

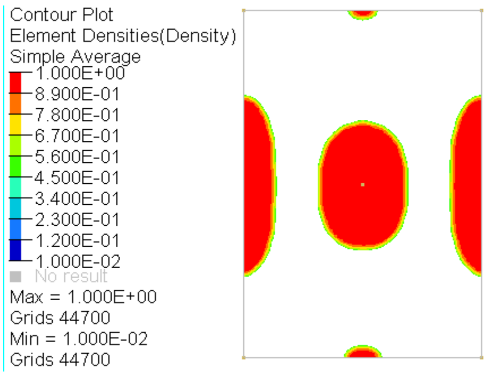

Fig. 2 Optimization result of strengthening material density

2.2 Test setup

The vented gas explosion tests were carried out in a RC chamber with the internal dimensions of 3 m × 2 m × 2 m, as shown in Fig. 3. There are two openings on the walls of the chamber. The small opening of 0.8 m × 0.8 m was used to install vent covers and acted as a vent window. The larger opening with dimensions of 3 m × 2 m was used to place wall specimens for explosion testing.

The methane was piped into the chamber from a group of cylinder gas tanks, which was placed about 150 meters away. As shown in Fig. 3(a), an explosion-proof fan (CBF-300, Zhejiang Dafeng Blowers, China) was installed in the chamber to ensure homogeneity of the mixtures of gases. An infrared gas analyzer (QGS-08C, Nanjing Xinfen, China) was employed to monitor the methane concentration. An igniting pill was hung at the center of the chamber to fire the flammable gas mixtures.

Four piezo-resistive pressure sensors (CYG1409, Kunshan Shuangqiao, China) were mounted inside the chamber to record the explosion overpressure. The pressure sensors have a measuring range of -20 to 150 kPa with the accuracy of 0.5%. Owing to the high temperature inside the chamber during the explosions, all pressure sensors were equipped with water-cooling circulation systems to protect the sensors. Six displacement transducers (WYJL, Xian Xinmin, China) were mounted on the pre-made steel frame at an equal space of 750 mm to record the displacement-time histories of tested walls. The displacement transducers have the measuring range of 0-300 mm. A high-speed camera (FASTCAM SA-Z, Photron, Japan) that can capture images at 20,000 frames per second was triggered at about 100 meters away from the test wall to record the failure progress of the tested specimens. The signals of displacement transducers and pressure sensors were captured by the data acquisition system (DongHua 5927, Donghua Testing Technology Co., Ltd., China), which was sampled at a frequency of 30 kHz.

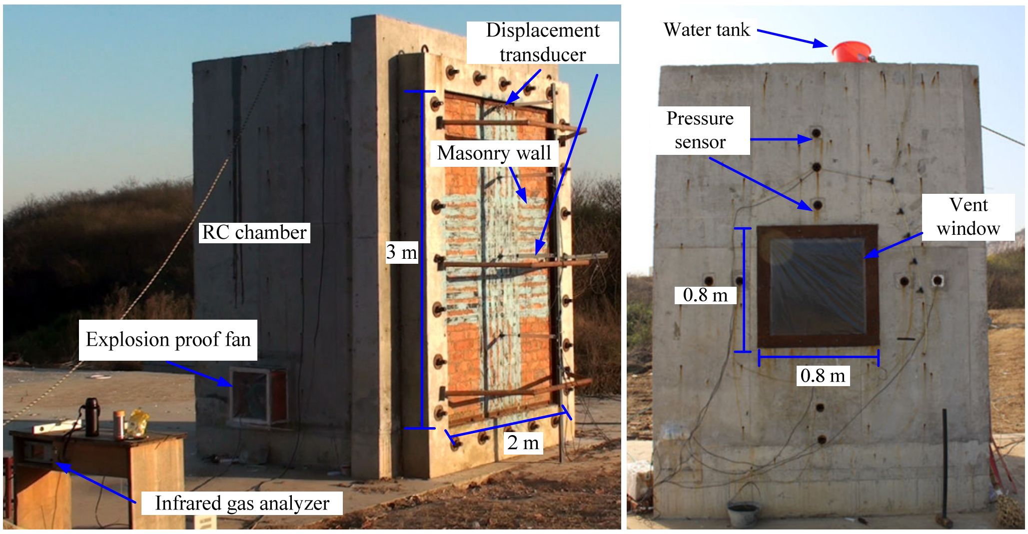

(a) Side view (b) Back view

Figure 3 Test setup

2.3 Test scheme

In this study, nine tests were conducted to investigate the performance of CFRP strip strengthened clay brick masonry walls under gas explosion loads, as listed in Table 1. The gas concentrations and vent covers were adjusted to achieve the desired gas explosion loads.

Table 1 Testing scheme

Test	Wall	Methane Concentration	Vent Cover
1	W1	11.5%	6μm film
2	W1	6.5%	4mm glass
3	W1	6.5%	4mm glass
4	W2	6.5%	4mm glass
5	W2	12.5%	10mm glass
6	W2	12.5%	12mm glass
7	W3	6.5%	4mm glass
8	W3	6.5%	5mm glass
9	W3	12.5%	10mm glass

2.4. Results and discussions

2.4.1 Vented gas explosion loads

In the previous study [23, 31, 32], it was reported that the overpressure inside the chamber was nearly uniformly distributed during vented gas explosions. The recorded pressure time histories from different pressure sensors in the current study also confirmed this observation. Therefore, only overpressure-time histories recorded by the pressure sensor P1 are reported in this study, as shown in Fig. 4. Pressure peaks and impulse are also summarized in Table 2. In general, four major overpressure peaks might be captured when a gas explosion occurs in a vented space [31]. As shown in Fig. 4, the number of peaks and peak values are different from each other owing to different explosion scenarios because methane concentrations, vent covers and the damage of the tested masonry walls all have significant influence on the overpressure load of vented gas explosion.

By comparing the overpressure-time histories of Test 2/3/4/7/8 with concentration 6.5%, it is found that the curves at the rising stage of pressure nearly overlap with each other. Similar results can be found by comparing the data of Test 5/6/9 with concentration 12.5%. These indicate that the gas concentration control is accurate, and the testing data are acceptable.

With the same test conditions (i.e. concentration 6.5% and vent cover 4mm glass panel), the rising stages of Test 2/3/4/7 agree well with each other while the peak values of Test 2/3/4/7 are 7.81 kPa, 10.12 kPa, 10.32 kPa and 8.73 kPa respectively. The difference of peak values may be caused by the variations in the strength of glass panels used as vent cover caused by random fluctuations of boundary conditions and material strength. Similar results were also observed by comparing the data of Test 5/9 with concentration 12.5% and vent cover 10 mm glass panel. The failure load and process of the vent cover affect the peak pressure that can be achieved in a vented explosion. In this study, the response and damage of each tested masonry wall are discussed with respected to the respective recorded pressure time histories.

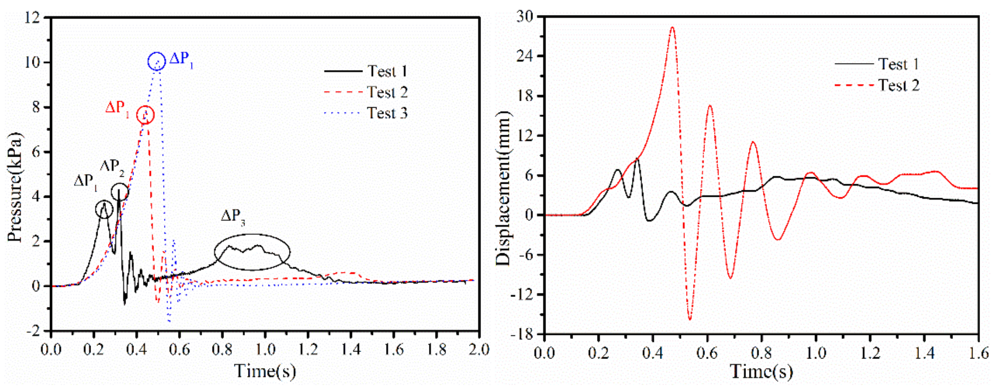

(a) Overpressure-time histories for W1 (b) Displacement-time histories for W1

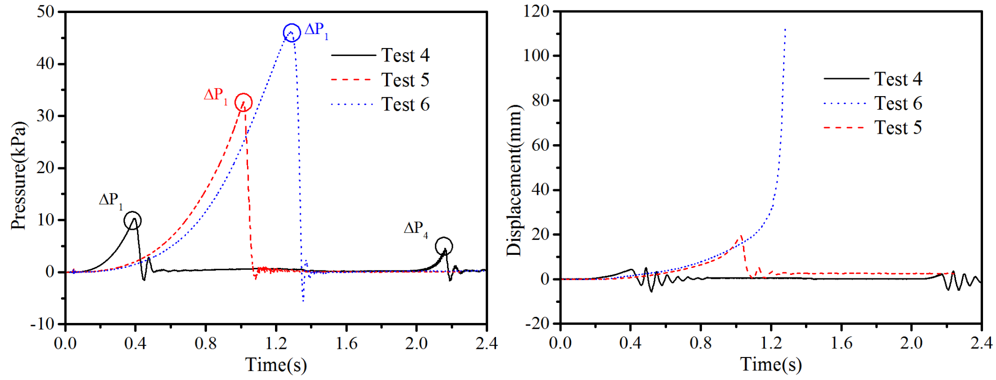

(c) Overpressure-time histories for W2 (d) Displacement-time histories for W2

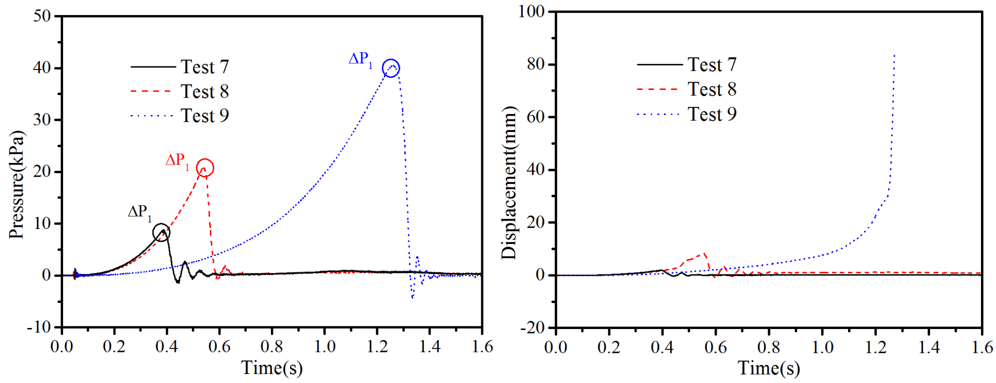

(e) Overpressure-time histories for W3 (f) Displacement-time histories for W3

Fig. 4 Test results of wall specimens

Table 2 Summary of testing results

Test	Wall	ΔP Peak (P: kPa)	Duration (ms)	Impulse (I: kPa·s)	Maximum displacement (D: mm)	P/D (kPa/mm)	Residual displacement (mm)
1	W1	3.77	297	1.33	6.88	0.548	0
2		7.83	495	1.43	28.43	0.275	2.32
3		10.12	555	1.96	—	—	Collapse
4	W2	10.32	400	1.27	4.38	2.356	0.0
5		32.79	1027	9.08	19.51	1.681	2.55
6		46.16	1303	17.85	—	—	Collapse
7	W3	8.73	388	1.13	1.90	4.595	0.0
8		20.93	538	3.48	8.17	2.574	1.08
9		40.45	1283	14.46	—	—	Collapse

2.4.2 Displacement-time histories

The mid-span displacement-time histories of wall specimens in each test are shown in Fig. 4 and the maximum and residual displacements of wall specimens are also given in Table 2.

The effect of strengthening methods on the elastic response of wall specimens is studied by comparing the data of Test 1/4/7. In these three tests, the wall specimens experienced elastic response without residual displacement after tests. The ratio of P/D (i.e. the ratio of peak pressure over maximum displacement) is used as an indicator to assess strengthening performance. As shown in Table. 2, the P/D ratios of unstrengthened wall specimen W1, wall specimen W2 strengthened with CFRP distributed layout and wall specimen W3 strengthened with CFRP concentrated layout are 0.548, 2.356 and 4.595, respectively. As compared with the unstengthened wall specimen, the P/D ratios of the strengthened wall specimens with distributed layout and concentrated layout increase by 329% and 739%, respectively. These are because of the increase in structural stiffness owing to the change of boundary conditions through anchoring the FRP strips to the supporting frame, as well as the existence of CFRP strips. Obviously, the concentrated layout is more effective than the distributed layout at improving the specimen stiffness. It is because the concentrated layout is more effective than the distributed layout in enhancing the equivalent section area and structural stiffness in central area.

The effect of strengthening methods on the inelastic response of wall specimens is studied by comparing the testing data of Test 2/5/7. Under the same test conditions (i.e. concentration 6.5% and vent cover 4 mm glass panel), the maximum displacement of W1 is 28.43 mm, which is 5.5 times higher than that of W2 and 14 times higher than that of W3. After testing, the wall specimen W1 experienced 2.32 mm residual displacement while no residual displacement was found for W2 and W3, which indicate that strengthening measures improved the resistance capacity of wall specimens significantly. In this study, Test 9 of wall specimen W3 had the same test condition as Test 5 (i.e. concentration 12.5% and vent cover 10mm glass panel). The wall specimen W3 collapsed but W2 did not due to the unexpected intensive gas explosion loads in test 9, i.e. 32.79 kPa vs 40.45 kPa peak load, and 9.08 kPa.s vs 14.46 kPa.s impulse, which was caused by the higher venting pressure owing to the higher strength of the venting glass panel.

2.4.3 Failure modes of wall specimens

The failure process of the tested specimens was recorded by the high-speed camera, as shown in Fig. 5. Fig. 5 (a) shows the unstrengthened specimen W1 experienced a horizontal crack in the mid-span area before the collapse of the wall. This might be attributed to the fact that for the unstrengthened one-way specimen under uniformly distributed loads, the maximum bending moment occurs at the mid-span area and cracks form along the masonry-mortar interface due to their low tensile strength. With the increase of overpressure inside the chamber, W1 collapsed and was divided into two sections along the horizontal crack in the mid-span area. The specimen W2 strengthened with distributed layout experienced more small cracks and behaved like a typical two-way slab under bending. With the increase of internal overpressure, W2 was broken into small pieces. Similar to W2, W3 strengthened with concentrated layout also experienced typical two-way bending failure under vented gas explosions. The failure mode changed from one-way of unstrengthened specimen to two-way of strengthened specimens because of the change of boundary conditions by anchoring the FRP strips to the concrete frame. As shown in Fig. 6, some bricks were found at the corners of RC frame after the strengthened wall specimens W2 and W3 collapsed, which might be due to the arching effect. In addition, the rupture of CFRP strips were observed along the edges and in the mid-span area as shown in Fig. 7.

(a) W1 (Test 3)

(b) W2 (Test 6)

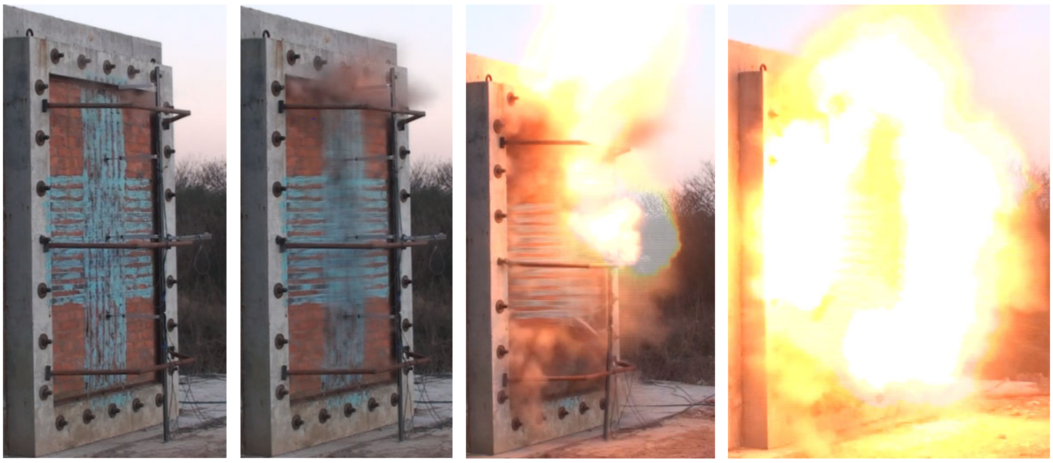

(c) W3 (Test 9)

Fig. 5 Failure progress of the tested walls

(a) Unstrengthened (b) Distributed layout (c) Concentrated layout

Fig. 6 Views of wall specimens after testing

(a) Edges (b) Mid-span area

Fig. 7 Rupture of CFRP strips

3 Numerical study

3.1 Numerical model

3.1.1 Material model

In order to determine the brick and mortar material parameters, a series of laboratory tests were conducted according to the testing standards i.e. GB/T 2542-2012 and JGJ/T70-2009 [33, 34]. The mean uniaxial compressive strength of clay brick and mortar were 7.53 MPa and 14.67 MPa, respectively. The anisotropic material model *Mat_96 (MAT BRITTLE DAMAGE) in LS-DYNA was employed to model the bricks and mortar. The compressive yield strength was taken from the material tests. The density and Young's modulus of brick and mortar were also acquired from the material tests. The Poisson's ratio, tensile limit, shear limit, fracture toughness and shear retention factor were obtained from the references [24, 35, 36]. The parameters used in the numerical simulations are listed in Table 3.

Table 3 Material parameters of clay brick and mortar [24, 35, 36]

	Density (kg/m^3)	Young's Modulus (MPa)	Poisson's Ratio	Compressive Yield Stress (MPa)	Tensile Limit (MPa)	Shear Limit (MPa)	Fracture Toughness (N/m)	Shear Retention Factor
Brick	1150	380	0.15	7.5	3.0	3.0	120	0.03
Mortar	2100	4644	0.25	14.7	5.0	7.0	140	0.03

The isotropic material model *Mat_3 (MAT PLASTIC KINEMATIC) was used to model the unidirectional CFRP strips. Without defining the kinematic hardening plasticity, CFRP strips were simplified as an isotropic and elastic-brittle material, which is a cost-effective method to simulate the CFRP strips. Quasi-static test was carried out to investigate the mechanical properties of CFRP strip by using universal testing machine, as shown in Fig. 8. The CFRP specimens were prepared and tested according to the guidelines [37, 38]. The parameters of CFRP material are listed in Table 4.

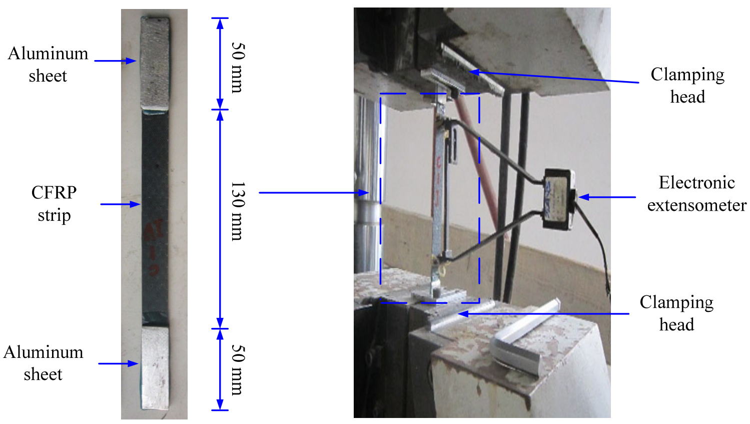

Fig. 8 Quasi-static test of CFRP strip

Table 4 Material parameters of CFRP

	Density (kg/m^3)	Young's Modulus (GPa)	Poisson's Ratio	Tensile Strength (MPa)	Thickness (mm)	Failure Elongation %
CFRP	1800	212	0.17	4100	0.167	1.74

3.1.2 Geometric model and modelling strategy

In this study, the masonry wall was simulated by the detailed micro model using commercial software LS-DYNA. The mortar and bricks were modeled individually and the nodes along the interfaces between the mortar and bricks are merged. The dimensions of wall models with thickness of 115 mm, 3.0 m height and 2.0 m width are shown in Fig. 9. The size of bricks is 240×115×90 mm and the thickness of mortar joints is 5 mm.

Bricks and CFRP strips were meshed with the element size of 20 mm and mortar was meshed into two layers after conducting mesh convergence test. Solid 164 (with element formulation of constant stress solid element) was used for solid elements of bricks and mortar. Shell 163 (with element formulation of Belytschko-Tsay) was used for angle irons and CFRP strips. The finite element model had a total of 145,900 solid elements and 7,770 shell elements for the masonry and CFRP strips, respectively.

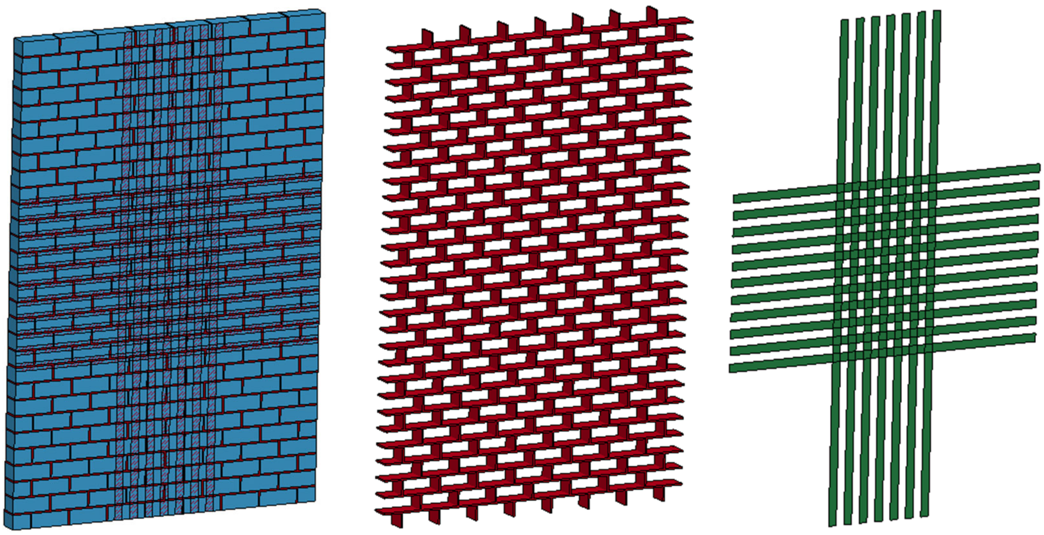

(a) Full wall model (b) Mortar model (c) CFRP strip model

Fig. 9 Finite element models of strengthened masonry walls with concentrated layout

The bonding between CFRP strips and masonry walls was simulated as a tie-break contact in the numerical model. In LS-DYNA, the tie-break contact is governed by the stress-based failure criterion as follows,

$$\left(\frac{|\sigma_n|}{f_n}\right)^2 + \left(\frac{|\tau_s|}{f_s}\right)^2 \geq 1 \qquad (1)$$

where σ_n and τ_s represent the normal stress and shear stress on the contact surface, respectively; f_n and f_s represent the normal failure stress and shear failure stress, respectively. In this study, the static and dynamic coefficients of friction were 0.7. The normal failure stress f_n and shear failure stress f_s were 42 MPa and 2 MPa, respectively. The above parameters were determined from the testing report of epoxy resin provided by the supplier and calibrated with the testing data of Test 5 by trial and error approach.

According to the testing setup, the boundary conditions applied in the numerical models are shown in Fig. 10. The RC frame was included in the model and simplified as elastic solid elements. For the unstrengthened walls, the interfaces between the RC frame and the masonry wall were simulated as tie-break contact. The static and dynamic coefficients of friction for the top and bottom edges were defined as 0.7 and the normal failure stress f_n and shear failure stress f_s were set as 7 MPa and 1 MPa, respectively. For the strengthened walls, the static and dynamic coefficients of friction of the left and right boundaries were set as 0.7. The normal failure stress f_n and the shear failure stress f_s were defined as 7 MPa and 1 MPa, respectively. The angle irons were also modelled along the boundary. The surface to surface contact was defined between the angle iron and the masonry walls and the contact between CFRP and angle irons. The relevant parameters were calibrated with the testing data of Test 2 and Test 5.

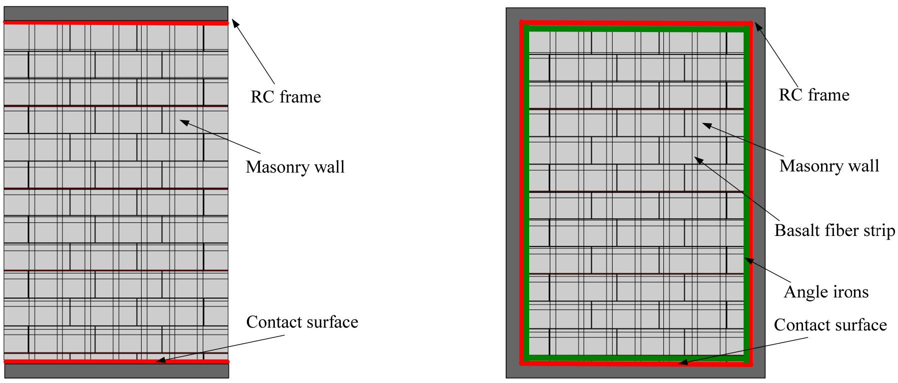

(a) Unstrengthened wall (b) Strengthened wall

Fig. 10 Boundary conditions of wall models

3.2 Model calibration

Applied with the pressure time history recorded from experiments, the numerical models of masonry wall are calibrated with the testing data. The numerical predictions and testing data of three walls under test 2/5/6/8/9 are compared in Fig. 11. As shown in Fig. 11(a), the predicted period of vibration and the peak value of mid-span displacement of the specimen W1 agree well with the testing data. As for the strengthened wall specimens W2 and W3, the predicted mid-span displacement histories also agree well with the testing data. For instance, in Test 5, the predicted peak displacement is 18.72 mm, which is about 4.3 % less than the testing data of 19.53 mm. In Test 8, the prediction of 8.05 mm is 1.9 % less than the testing data of 8.20 mm. The damage modes of the specimens are also compared. As shown in Fig. 12 and Fig. 13, the damage modes and the yield lines of wall specimens W1 and W2 can be well predicted. Therefore, it can be concluded that the numerical model developed in this study can give good predictions of structural response of unstrengthened and strengthened clay brick masonry walls against vented gas explosions.

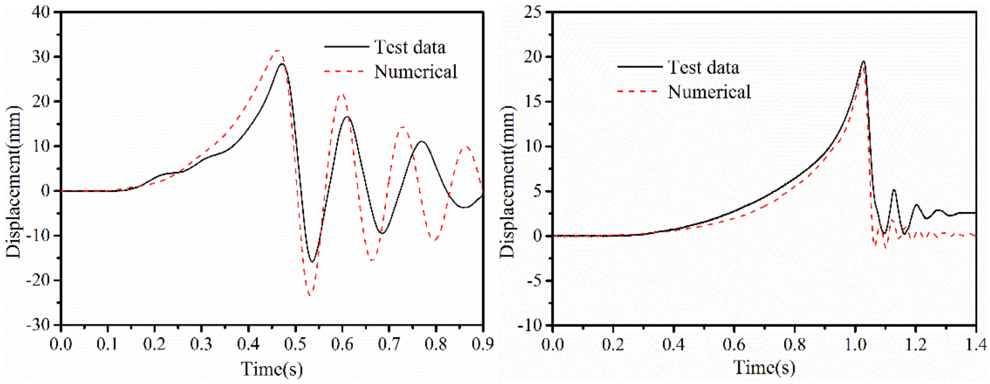

(a) Test 2 (b) Test 5

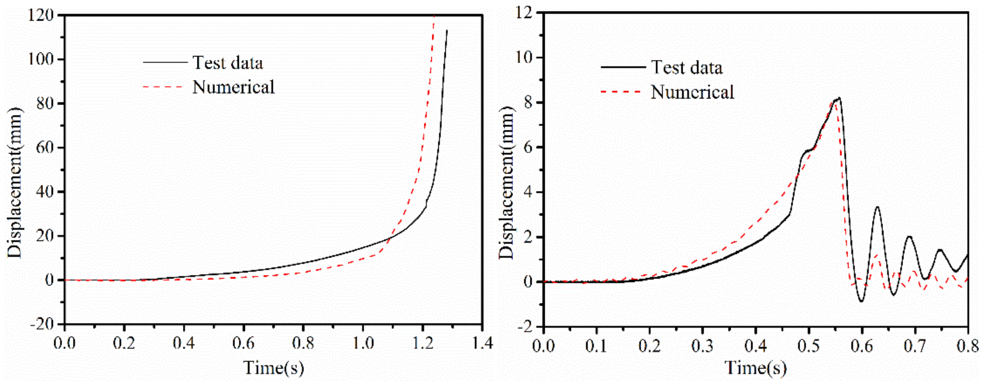

(c) Test 6 (d) Test 8

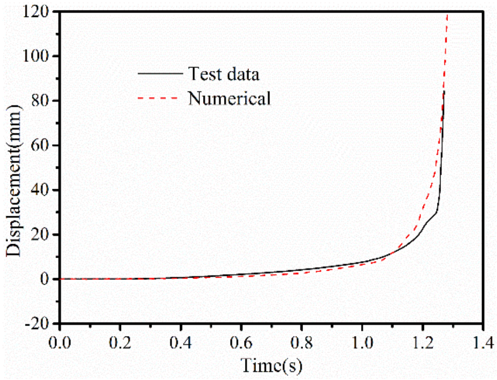

(e) Test 9

Fig. 11 Comparison of mid-span displacement between numerical predictions and testing data

t=480 ms t= 520ms t= 560ms t=600 ms

(a) Test observations

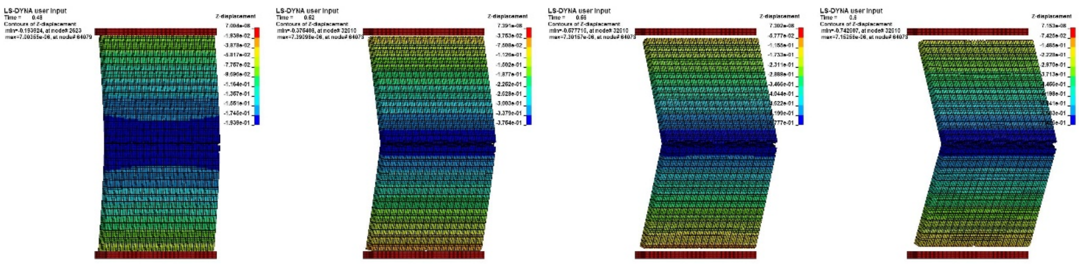

t=480 ms t= 520ms t= 560ms t=600 ms

(b) Numerical predictions

Fig. 12. Failure modes of wall specimen W1 (Test 3)

(a) Test observations

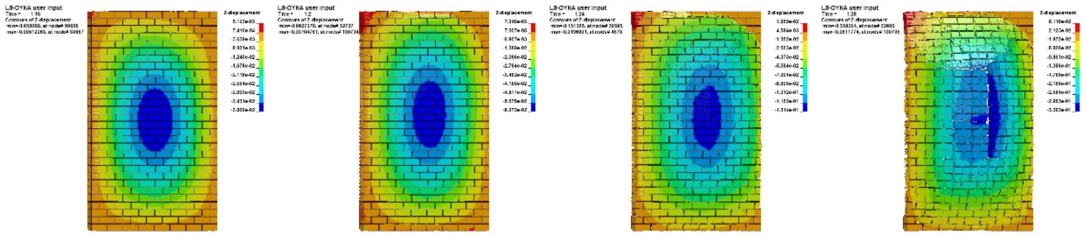

t= 1160 ms t= 1200 ms t= 1240 ms t= 1280 ms

(b) Displacement contour of wall specimen

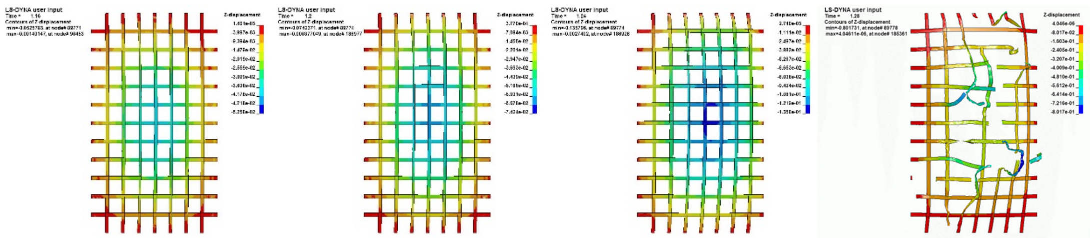

t= 1160 ms t= 1200 ms t= 1240 ms t= 1280 ms

(c) Displacement contour of CFRP strips

Fig. 13. Failure modes of wall specimen W2 (Test 6)

3.3 Parametric studies

In this section, the performances of the unstrengthened clay brick walls with different thicknesses and heights are compared under various blast loads specified by design codes. In addition, the strengthening effectiveness of using CFRP, GFRP and spray-on polyurea are compared under blast loads. The simplified blast loads used for structural design against gas explosion [39-41] are adopted in the analyses and shown in Fig. 14. Blast load A has the overpressure of 21 kPa and the duration of 100 ms, which corresponds to the explosion of 6% ethane cloud with the diameter of 60 m and 4m-height detonated at a distance of 75 m. The overpressure and duration of blast load B are 69 kPa and 20 ms, which corresponds to a 1000 kg TNT equivalency at a distance of 30.5 m. Only blast load B is investigated in the parametric studies as masonry wall experiences more severe damage under blast load B. In addition, damage criteria need to be defined to classify damage level of masonry walls. The support rotation limit used to classify damage level (i.e. reusable and non-reusable) of masonry walls [42] is employed in this study as given in Table 5. In addition, the failure criterion defined for unstrengthened wall is the mid-span displacement exceeding the wall thickness in [42]. In this study, the strengthened wall is defined as failed when the retrofitting materials fracture, and simultaneously the mid-span displacement exceeds the wall thickness.

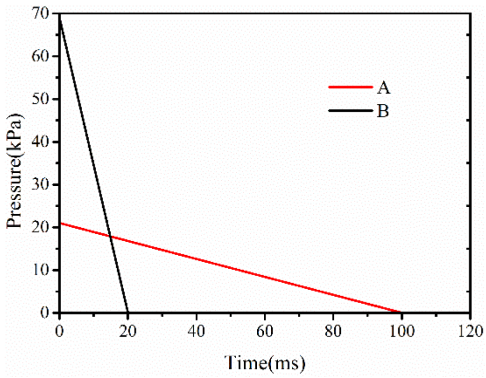

Fig. 14 Design blast loads [39]

Table 5 Damage criteria for masonry walls [42]

Damage level	Wall type	Support rotation limit
Reusable	One-way	0.5°
	Two-way	0.5°
Non-reusable	One-way	1.0°
	Two-way	2.0°

3.3.1 Brief description of numerical models

The dimension of wall models used for parametric studies is 1.0 m in width and three wall heights (i.e. 3 m, 4 m and 5 m) are considered. The size of bricks is 240 mm × 115 mm × 90 mm and the thickness of mortar is 10 mm. Three wall thicknesses (i.e. 115 mm, 240 mm and 365 mm) are considered as shown in Fig. 15. It should be noted that only one-way wall is considered in the current parametric study. Three composite materials (i.e. CFRP strip, GFRP strip and spray-on polyurea) are used in the parametric study and the mechanical properties of composite materials are listed in Table 6. As shown in Fig. 16, the vertical FRP (i.e. CFRP and GFRP) strips are distributed at a distance of 250 mm along the horizontal direction of masonry walls and the width of FRP strips is 50 mm. The spray-on polyurea is applied on the whole back face of masonry walls.

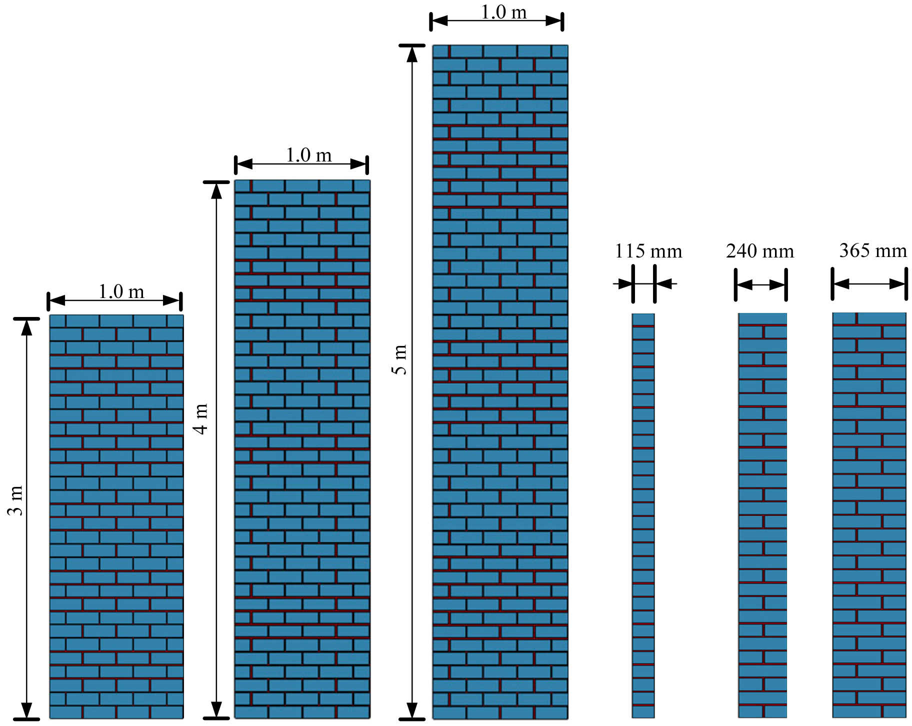

Fig. 15 Wall models used for parametric studies

Table 6 Mechanical properties of FRPs and spray-on polyurea [26, 43]

Material	Density (kg/m^3)	Thickness (mm)	Ultimate tensile strength (MPa)	Young's modulus (GPa)	Ultimate strain (%)
CFRP	1800	0.167	4100	212.0	1.74
GFRP	2400	0.125	3040	73.0	4.16
Spray-on polyurea	1150	--	13.29	0.229	113

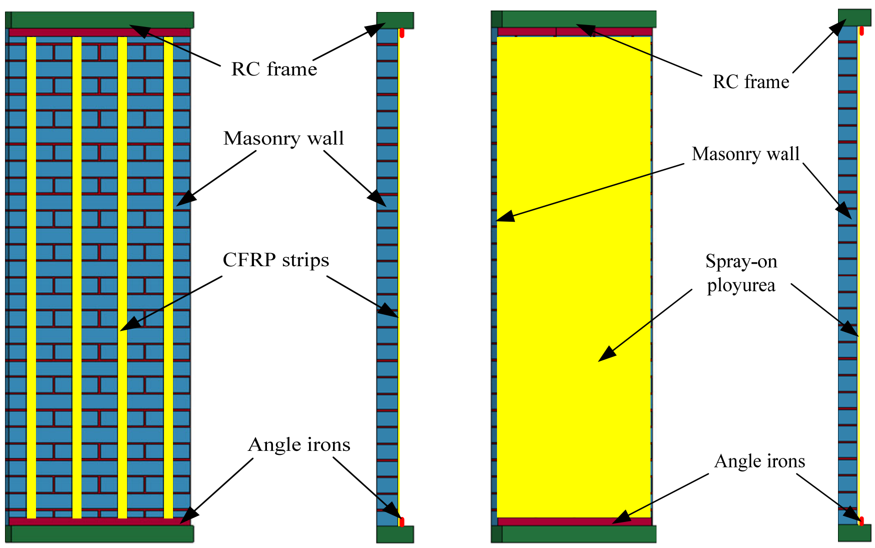

(a) FRP strengthened walls (b) Spray-on polyurea strengthened walls

Fig. 16 Strengthened wall models used for parametric studies

3.3.2 Performance of unreinforced masonry walls under specified blast loads

In this section, the performances of unstrengthened clay brick masonry walls under specified blast loads are studied. Nine wall models are built with varying wall thicknesses and heights subjected to Load B. The damage levels of unstrengthened masonry walls under Load B are listed in Table 7, it is found that the walls with the thickness of 240 mm and 365 mm survive by experiencing the damage level of either non-reusable or reusable, while the walls with the thickness of 115 mm collapse. Therefore, the strengthening measures are needed to prevent the 115mm-thick masonry walls from collapse. The maximum displacement time histories of unreinforced masonry walls under Load B are also compared as shown in Fig. 17. It is found that with the increase of wall thickness and the decrease of wall height, the maximum displacement and damage level of masonry walls decrease significantly. Taking the 3m-high walls as examples, the masonry wall with the thickness of 115 mm collapses. The walls with the thickness of 240 mm and 365 mm experience reusable damage and no-damage respectively and the maximum displacements are 23.93 mm and 11.15 mm, respectively. Similar conclusion can be drawn by comparing the damage levels and the maximum displacements of masonry walls with the height of 4 m and 5 m. When the wall thickness is 240 mm, the maximum displacements of walls with the height of 3 m, 4 m and 5 m are 23.9 mm, 46.8 mm and 99.8 mm, respectively and the corresponding damage levels are reusable, non-reusable and non-reusable, respectively. Increasing the wall thickness increases the inertia resistance and the stiffness of the wall, and reducing the height of the wall also increases the stiffness as well. What is more, with the decrease of slenderness ratio (wall height over thickness), the arching action of masonry walls increases.

The failure modes of the 115 mm-thick walls with different heights are shown in Fig. 18. When the wall height is 3 m or 4 m, the masonry walls experience flexural bending and the maximum displacement of walls occurs in the mid-span area. The walls break into two large pieces with the formed horizontal crack. When the height increases to 5 m, the maximum displacement of walls also occurs in the mid-span area but two horizontal break lines are generated and divide the walls into three major pieces.

Table 7 Result summary of unreinforced walls under blast load B

Wall thickness	Wall height		
	3m	4m	5m

115 mm	Failed	Failed	Failed
240 mm	Reusable	Non-reusable	Non-reusable
365 mm	No damage	Reusable	Reusable

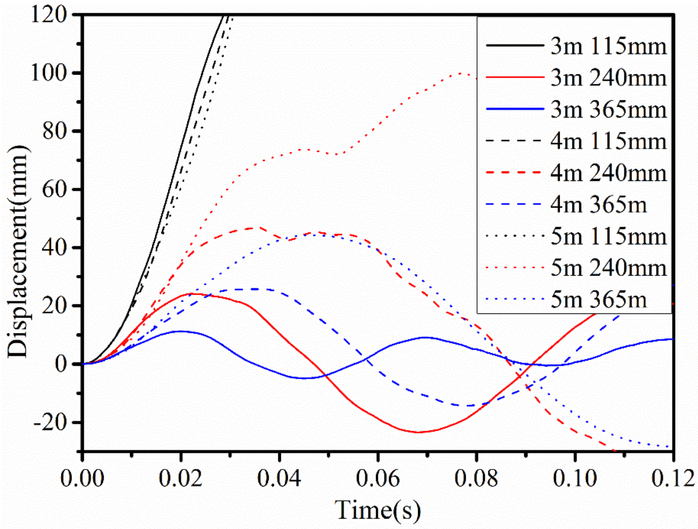

Fig. 17 Comparison of displacement time histories

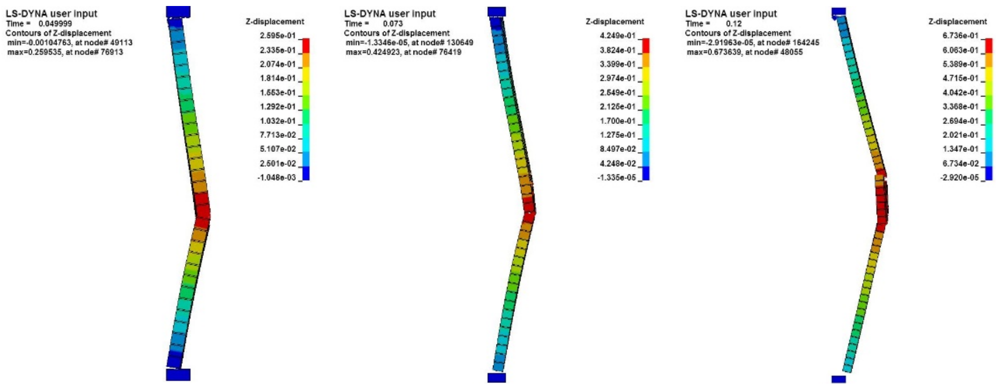

(a) 3 m (b) 4 m (c) 5 m

Fig. 18 Failure modes of unstrengthened walls with various heights

3.3.3 Effectiveness of Strengthening

The strengthening methods of masonry walls by using three composite materials (i.e. CFRP strip, GFRP strip and spray-on polyurea) are compared and discussed in this section. With the strengthening layouts as shown in Fig. 16, the thicknesses of composite materials are determined to prevent the collapse of 115 mm-thick masonry walls as listed in Table 8. It is found that with the increase of wall height, more strengthening materials is required to prevent masonry wall collapse. For example, the CFRP strips used for strengthening the 115 mm-thick walls with the height of 3 m, 4 m and 5 m are 1 layer, 2 layers and 4 layers, respectively. The masonry walls strengthened by the spray-on polyurea experience typical flexural behavior and the profiles at the maximum deflection are shown in Fig. 19.

The behaviors of 3m-high masonry walls strengthened by three composite materials at the maximum deflection are compared in Fig. 20. It is observed that the spray-on polyurea strengthened wall experiences the largest displacement (285.5 mm), followed by the GFRP strengthened wall (207.8 mm) and the CFRP strengthened walls (140.1 mm). CFRP strips show the best strengthening effectiveness in term of maximum mid-span displacement. This is because of the differences of strengthening composites (i.e. cross section area, Young's modulus and ultimate strain). Compared with the spray-on polyurea, FRP materials have higher Young's modulus and lower ultimate strain. Externally bonding FRP materials onto the surface of masonry walls enhances the stiffness of walls more effectively when the response of walls is within elastic range. Applying spray-on polyurea has very limited effect on the increase of wall stiffness. However, with the accumulation of wall deformation, the tensile membrane effect of the spray-on polyurea strengthened masonry walls becomes more and more significant due to the higher ultimate strain of polyurea and in turn improve the resistance of masonry walls. As shown in Fig. 21, the spray-on polyurea strengthened masonry walls also experience typical one-way flexural failure. The plastic strain of masonry concentrates in the mid-span area due to the flexure damage and along the edges caused by the arching effect. The plastic strain of spray-on polyurea is also observed in the mid-span area and along the edges which are caused by the tension after cracking of the masonry walls and the membrane effect of structures.

Table 8 Strengthening suggestions for the 115mm-thick masonry walls

Material	Wall height		
	3m	4m	5m
CFRP	1 layer	2 layers	4 layers
GFRP	2 layers	4 layers	5 layers
Spray-on polyurea	2 mm-thick	4 mm-thick	5 mm-thick

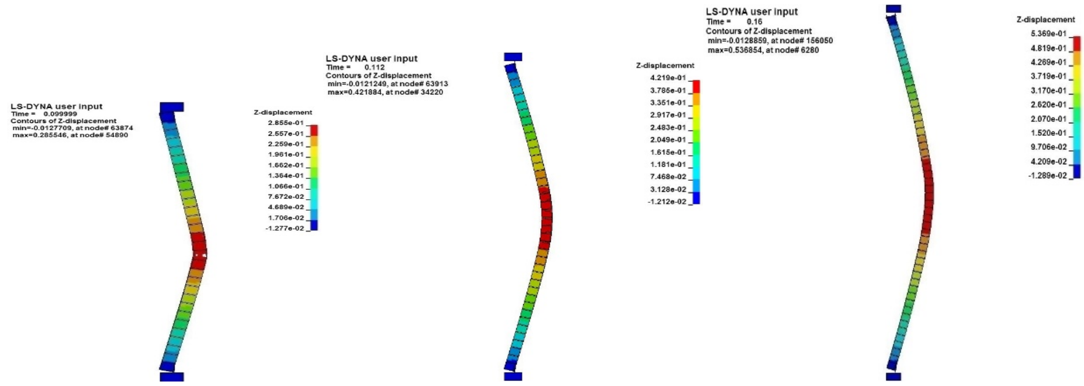

(a) 3m (b) 4m (c) 5m

Fig. 19 Performance of spray-on polyurea strengthened walls at the maximum deflection moment

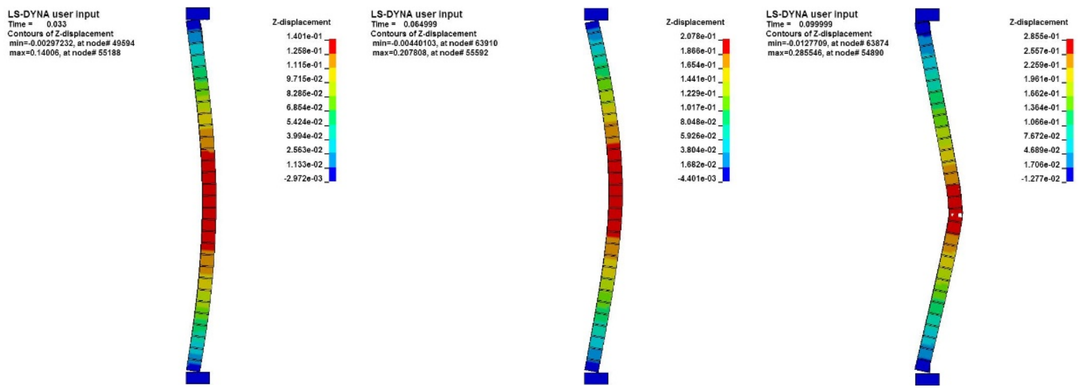

(a) 1 layer CFRP strip (b) 2 layer GFRP strip (c) 2 mm-thick spray-on polyurea

Fig. 20 Behavior of strengthened masonry walls

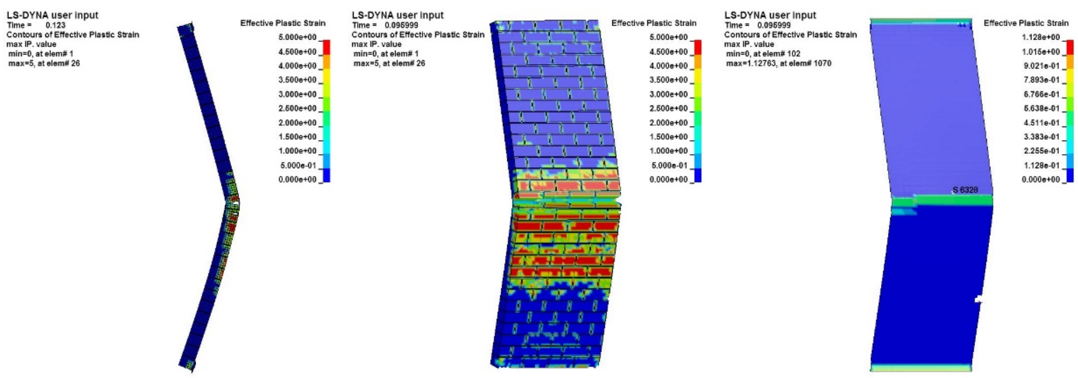

(a) Side view (b) Plastic strain of masonry (c) Plastic strain of polyurea

Fig. 21 Failure mode of spray-on polyurea (1 mm-thick) strengthened masonry walls

4 Conclusions

In this paper, the performances of CFRP strip strengthened clay brick masonry walls under vented gas explosions were investigated by conducting full-scale field tests and numerical simulations. As observed from the tests, the unstrengthened masonry walls changed the response and damage modes from typical one-way to two-way after strengthening. The CFRP strips of strengthened specimens experienced rupture at the edges and mid-span area. The concentrated layout was more effective in improving the blast resistant capacity than the distributed layout. Detailed micro models of masonry walls were developed, and the accuracy of numerical models were validated with testing data. With the calibrated numerical model, it was found that the maximum displacement and damage level of masonry walls decreased significantly with the increase of wall thickness or the decrease of wall height. 115 mm-thick masonry walls needed be strengthened to prevent collapse. With the increase of wall height, more strengthening materials were required to prevent wall collapse. The strengthening solutions by using CFRP, GFRP and spray-on polyurea were suggested to strengthen 115 mm-thick masonry walls. The spray-on polyurea enhanced the tensile membrane effect and the blast resistance of strengthened masonry walls due to the higher ultimate strain. As compared to spray-on polyurea, bonding FRP materials externally on the surface of masonry walls enhanced the stiffness of walls more effectively when the response was in the elastic range and improved the resistance of walls due to the arching effect. In term of maximum displacement, CFRP strips showed the best strengthening efficacy among the three strengthening materials because of its higher modulus and strength.

Acknowledgement

The authors acknowledge the financial support from the National Basic Research Program of China (973 Program, Grant No. 2015CB058000) and the Australian Research Council (Grant No. LP150100259).

References

[1] J. Crawford, K. Morrill, Retrofit techniques using polymers and FRPs for preventing injurious wall debris, in: Fibre-Reinforced Polymer Reinforcement for Concrete Structures: (In 2 Volumes), World Scientific, 2003, pp. 1199-1208.

[2] P.A. Buchan, J.F. Chen, Blast resistance of FRP composites and polymer strengthened concrete and masonry structures – A state-of-the-art review, Composites Part B: Engineering, 38 (2007) 509-522.

[3] S.A. Hamoush, M.W. McGinley, P. Mlakar, D. Scott, K. Murray, Out-of-plane strengthening of masonry walls with reinforced composites, Journal of Composites for Construction, 5 (2001) 139-145.

[4] H. Hamilton Iii, C. Dolan, Flexural capacity of glass FRP strengthened concrete masonry walls, Journal of Composites for Construction, 5 (2001) 170-178.

[5] M.L. Albert, A.E. Elwi, J.R. Cheng, Strengthening of unreinforced masonry walls using FRPs, Journal of Composites for Construction, 5 (2001) 76-84.

[6] T.T. Bui, A. Limam, Out-of-plane behaviour of hollow concrete block masonry walls unstrengthened and strengthened with CFRP composite, Composites Part B: Engineering, 67 (2014) 527-542.

[7] Y.A. Al-Salloum, T.H. Almusallam, Load capacity of concrete masonry block walls strengthened with epoxy-bonded GFRP sheets, Journal of Composite Materials, 39 (2005) 1719-1745.

[8] H. Elsanadedy, Y. Al-Salloum, Z. Al-Zaheri, S. Alsayed, H. Abbas, Behavior and Design Aspects of FRP-Strengthened URM Walls under Out-of-Plane Loading, Journal of Composites for Construction, (2016) 04016048.

[9] T. Hrynyk, N. Galati, J.J. Myers, An analytical approach to predict the out-of-plane behavior of FRP retrofitted masonry infill walls with arching action, in: Proc., 3rd Int. Conf. Advanced Composites in Construction, 2007, pp. 320-327.

[10] T.D. Hrynyk, J.J. Myers, Out-of-plane behavior of URM arching walls with modern blast retrofits: Experimental results and analytical model, Journal of structural engineering, 134 (2008) 1589-1597.

[11] J.J. Myers, A. Belarbi, K.A. El-Domiaty, Blast resistance of FRP retrofitted un-reinforced masonry (URM) walls with and without arching action, The Masonry Society Journal, 22 (2004) 9-26.

[12] P. Carney, J.J. Myers, Shear and flexural strengthening of masonry infill walls with FRP for extreme out-of-plane loading, in: Proc., Architectural Engineering Institute Annual Meeting, 2003.

[13] G.S. Urgessa, A.K. Maji, Dynamic response of retrofitted masonry walls for blast loading, Journal of engineering mechanics, 136 (2009) 858-864.

[14] K.H. Tan, M. Patoary, Blast resistance of FRP-strengthened masonry walls. I: approximate analysis and field explosion tests, Journal of Composites for Construction, 13 (2009) 422-430.

[15] L. Chen, Q. Fang, J. Fan, Y. Zhang, H. Hao, J. Liu, Responses of masonry infill walls retrofitted with CFRP, steel wire mesh and laminated bars to blast loadings, Advances in Structural Engineering, 17 (2014) 817-836.

[16] L. Chen, Q. Fang, C. Jiang, J. Fan, H. Hao, Response and damage level of confined masonry walls to blast, Disaster Advances, 6 (2013) 380-394.

[17] L.C. Muszynski, M.R. Purcell, Use of composite reinforcement to strengthen concrete and air-entrained concrete masonry walls against air blast, Journal of Composites for Construction, 7 (2003) 98-108.

[18] J.S. Davidson, J.W. Fisher, M.I. Hammons, J.R. Porter, R.J. Dinan, Failure mechanisms of polymer-reinforced concrete masonry walls subjected to blast, Journal of Structural Engineering, 131 (2005) 1194-1205.

[19] J.S. Davidson, J.R. Porter, R.J. Dinan, M.I. Hammons, J.D. Connell, Explosive testing of polymer

retrofit masonry walls, Journal of Performance of Constructed Facilities, 18 (2004) 100-106.

[20] S.H. Alsayed, H. Elsanadedy, Z.M. Al-Zaheri, Y.A. Al-Salloum, H. Abbas, Blast response of GFRP-strengthened infill masonry walls, Construction and Building Materials, 115 (2016) 438-451.

[21] L.K.S. G.L. PEZZOLA, & G. HEGEMIER, Analysis methods for CFRP blast retrofitted reinforced concrete wall systems, 14th International Conference on Structures Under Shock and Impact, (2016).

[22] Q. Bao, Q. Fang, S. Yang, Y. Zhang, H. Xiang, L. Chen, Z. Li, Experimental investigation on the deflagration load under unconfined methane-air explosions, Fuel, 185 (2016) 565-576.

[23] Q. Bao, Q. Fang, Y. Zhang, L. Chen, S. Yang, Z. Li, Effects of gas concentration and venting pressure on overpressure transients during vented explosion of methane–air mixtures, Fuel, 175 (2016) 40-48.

[24] Z. Li, L. Chen, Q. Fang, H. Hao, Y. Zhang, H. Xiang, W. Chen, S. Yang, Q. Bao, Experimental and Numerical Study of Unreinforced Clay Brick Masonry Walls Subjected to Vented Gas Explosions, International Journal of Impact Engineering, 104 (2017) 107-126.

[25] Z. Li, L. Chen, Q. Fang, H. Hao, Y. Zhang, W. Chen, H. Xiang, Q. Bao, Study of autoclaved aerated concrete masonry walls under vented gas explosions, Engineering Structures, 141 (2017) 444-460.

[26] Z. Li, L. Chen, Q. Fang, W. Chen, H. Hao, Y. Zhang, Experimental and numerical study of basalt fiber reinforced polymer strip strengthened autoclaved aerated concrete masonry walls under vented gas explosions, Engineering Structures, 152 (2017) 901-919.

[27] Ministry-of-Construction-of-the-PR-China, Code for design of masonry structures (GB50003-2011), China Architecture and Building Press, Beijing, China, 2011.

[28] OptiStruct 10.0 user's guide, Altair Engineering, Inc., 2009.

[29] M.P. Bendsøe, N. Kikuchi, Generating optimal topologies in structural design using a homogenization method, Computer Methods in Applied Mechanics and Engineering, 71 (1988) 197-224.

[30] R. Taylor, J. Thomas, N. Mackaron, S. Riley, M. Lajczok, Detail Part Optimization on the F-35 Joint Strike Fighter, in: 47th AIAA/ASME/ASCE/AHS/ASC Structures, Structural Dynamics, and Materials Conference, American Institute of Aeronautics and Astronautics, 2006.

[31] M. Cooper, M. Fairweather, J. Tite, On the mechanisms of pressure generation in vented explosions, Combustion and Flame, 65 (1986) 1-14.

[32] W. Mercx, C. Van Wingerden, H. Pasman, Venting of gaseous explosions, Process Safety Progress, 12 (1993) 40-46.

[33] General Administration of Quality Supervision Inspection and Quarantine of PR China, Test methods for wall bricks (GB/T 2542-2012), Standards Press of China, Beijing, China, 2012.

[34] Ministry of Construction of the PR China, Standard for test method of performacnce on building mortar (JGJ/T70-2009), China Architecture and Building Press, Beijing, China, 2009.

[35] S. Govindjee, G.J. Kay, J.C. Simo, Anisotropic modelling and numerical simulation of brittle damage in concrete, International Journal for Numerical Methods in Engineering, 38 (1995) 3611-3633.

[36] J. Halquist, LS-DYNA keyword user's manual version 971, Livermore Software Technology Corporation, Livermore, CA, 2007.

[37] A.D. 7565-10, Standard Test Method for Determining Tensile Properties of Fiber Reinforced Polymer Matrix Composites Used for Strengthening of Civil Structures, in, 2010.

[38] A.D. 3039-14, Standard Test Method for Tensile Properties of Polymer Matrix Composite Materials, in, 2014.

[39] W.L. Bounds, Design of blast-resistant buildings in petrochemical facilities, ASCE Publications, 2010.

[40] CIA1992, An Approach to the Categorisation of Process Plant Hazard and Control Building Design, Chemical Industies Association, London, England, 1992.

[41] SG-22, Siting and Construction of New Control Houses for Chemical Manufacturing Plants, Manufacturing Chemists Association, Washington, DC, 1978.

[42] Department of Defense, Structures to resist the effects of accidental explosions, United Facilities Criteria (UFC) 3-340-02, in, 2008.

[43] M. Irshidat, A. Al-Ostaz, A.-D. Cheng, C. Mullen, Nanoparticle reinforced polymer for blast protection of unreinforced masonry wall: laboratory blast load simulation and design models, Journal of Structural Engineering, 137 (2010) 1193-1204.